ORIGINAL

Orthotropic mechano-sorptive creep behavior of Chinese fir during moisture desorption process determined in tensile mode

Hui Peng[1,2] · Jiali Jiang[1] · Jianxiong Lu[1] · Jinzhen Cao[2]

Abstract

Time-dependent creep behavior is one of the most important material characteristics in wood products exposed to various environmental conditions. The creep behaviors, including the general viscoelastic creep (VEC) at constant moisture content and the mechano-sorptive creep (MSC) during moisture content variations, are, however, not sufficiently described. Given the anisotropy of wood, comprehensive data on the creep behavior will require knowledge of its moisture-dependent properties in relation to the three principal axes of anisotropy. The present study examined the tensile orthotropic creep behaviors of Chinese fir (*Cunninghamia lanceolata*): VEC at constant moisture content and MSC during desorption process, at 0, 20, 40, and 60% relative humidity (30 °C). The creep anisotropy of MSC was more pronounced than that of VEC. The free shrinkage caused the specimens to deform in the opposite direction to load in MSC tests. Based on the databases of free shrinkage, VEC, and MSC, it is obvious that the mechanical stress has a positive effect on MSC, which is presumed to be a result of the double effect composed of the rearrangement of hydrogen bonds and unstable state. The unstable state could be evaluated quantitatively by the mechano-sorptive strain. The mechano-sorptive strain of radial and tangential specimens is affected by the relative humidity to a higher degree than that of longitudinal specimens. Further, the unstable state exerted more influence on tangential specimens and less on longitudinal specimens.

✉ Jiali Jiang
jialiwood@caf.ac.cn

1 Research Institute of Wood Industry of Chinese Academy of Forestry, Hunan Collaborative Innovation Center for Effective Utilizing of Wood and Bamboo Resources, Beijing 100091, People's Republic of China

2 College of Materials Science and Technology, Beijing Forestry University, Beijing 100083, People's Republic of China

Introduction

The creep rate of wood is accelerated due to moisture content (MC) variations, i.e., the materials exhibit mechano-sorptive creep (MSC) (Hunt 1984; Holzer et al. 1989; Armstrong and Kingston 1960; Montero et al. 2012). Since deformation is usually the limiting factor in timber applications, any acceleration is evidently an important consideration. Given the distinctive anisotropy of wood, a complete creep characterization requires knowledge of the MSC properties related to the three principal axes of anisotropy (longitudinal L, radial R, and tangential T).

The MSC behavior was first described in the early 1960s for timber wood subjected to variable loading and humidity (Armstrong and Kingston 1960). Since then, a number of experiments have been carried out in order to investigate the complex MSC behavior. Most of them concern creep tests under variable humidity (Navi et al. 2002; Navi and Stanzl-Tschegg 2009; Huang 2016); in general, only few properties were tested for a given property–MC combination. In so far, comprehensive datasets comprising the MC-dependent orthotropic creep parameters are missing. While the creep behavior of wood in the L direction is relatively well known, the behavior perpendicular to the grain (G⊥) (i.e., in R and T direction) remains underexplored (Hering and Niemz 2012; Kaboorani et al. 2013; Peng et al. 2017). Since tensile stress G⊥ represents the weakest timber point, knowledge of this pattern, especially with regard to load capacity and failure prediction of wooden structures, is highly important. Although the creep behavior in R and T direction has been investigated by several authors (Takahashi et al. 2004, 2005; Jiang et al. 2016), data covering MC-dependent tensile MSC behavior are limited to a few references. Most notably, orthotropic creep parameters (especially those pertaining to MSC) are essential input parameters for advanced computational models used in modern civil engineering.

When wood is subjected simultaneously to load and MC variation below the fiber saturation point (i.e., MSC), the mechano-sorptive (MS) effect might dominate the MSC behavior. The MS effect contributes to the higher creep in either adsorption or desorption processes in comparison with the general viscoelastic creep (VEC) at constant MC. Generally, the MS effect is attributed to an unstable state in the wood cell wall under the external load when MC varies. The unstable state was the representation of moisture gradient and stress gradient in wood cell wall. When MC varied, the occurrence of moisture gradient and stress gradient may form "free volume" within the wood cell wall and disturb the equilibrium state of the molecular packing mode (Takahashi et al. 2004; Zhan et al. 2018). The MS effect may be observed as an additional deformation that cannot be measured directly because it is always accompanied by shrinkage or swelling and the VEC behavior. By applying the strain partition assumption (Muszyński et al. 2005, 2006; Saifouni et al. 2016), it is possible to mathematically generate the MS strain representing the MS effect. It has been assumed that the MSC strain is a sum of three phases, specifically: (1) swelling/shrinkage (ε_S) caused by MC variations, (2) VEC strain (ε_{ve}) corresponding to constant MC level and (3) MS strain (ε^{ms}) which arises from MS effect. Consequently, creep strain in wood under nonequilibrium MC is expressed as a linear superpositon.

$$\varepsilon = \varepsilon_s + \varepsilon_{ve} + \varepsilon^{ms} \tag{1}$$

To determine the magnitude of MS strain, the separation of strain components becomes the principal concern in the experimental design of creep. Quite frequently, only separation of the effect of free swelling/shrinkage is carried out, while the viscoelastic component (i.e., VEC) is neglected without proper justification (Navi et al. 2002; Saifouni et al. 2016; Peng et al. 2018).

In focus of the present study is the orthotropic MSC behavior in the course of decreasing MCs under relative humidity (RH) isohume (RHI) conditions. To obtain the MS strain induced by MS effect, the free shrinkage and VEC tests were conducted. The contribution of shrinkage, VEC, and MS effect on the orthotropic MSC during desorption process was expected to be quantitatively analyzed.

Materials and method

Materials

All the tests were performed on a 25-year-old Chinese fir. Without any visual defects and knots, clear wood specimens with L, R, and T grain orientations were cut to a size of 35 mm × 6 mm × 1.5 mm within the no. 6–14 growth rings (heartwood), see Fig. 1. The microfibril angle within no. 6 and no. 14 growth rings is about $13.26 \pm 0.49°$ and $12.92 \pm 0.65°$, respectively. The effects of MFA variation could thus be neglected. Specimens were divided into five groups by grain orientation to be conditioned at about 30 °C in climatic chambers at 0, 20, 40, 60, and 80% RH for more than 9 weeks until a constant mass was achieved. The 0, 20, 40, 60, and 80% RH conditions were attained via the humidification method over pentoxide or sulfuric acid (Peng et al. 2018), and the corresponding equilibrium MC (EMC) was about 0.6 ± 0.1, 3.5 ± 0.3, 6.0 ± 0.3, 9.3 ± 0.5, and $14.1 \pm 0.7\%$, respectively.
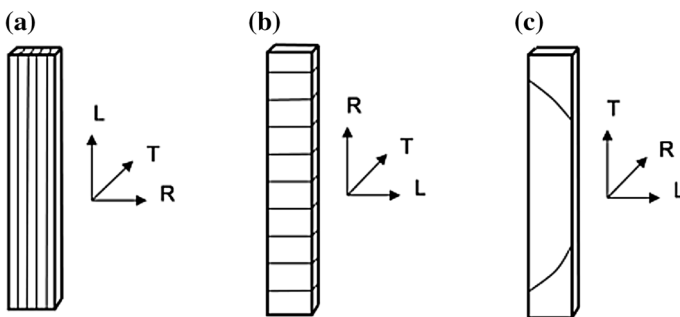

Fig. 1 Specimens in **a** L, **b** R, and **c** T grain orientation

Methods

Tensile mode with a distance of 17 mm was applied to a dynamic mechanical analyzer (DMA Q800, TA Instruments) equipped with a DMA-RH accessory (Fig. 2). The accessory controls the RH in the testing chamber precisely by modulating the mixture of dry nitrogen and saturated moisture. In order to eliminate the MC change during mounting of the sample, a specimen with a given EMC was first equilibrated for 60 min at the corresponding RH level in the DMA chamber. Afterward, RH decreased to the target RH. During these periods, the sample was kept in a straight position using a preload force of 0.01 N. Then, 420-min tests were carried out to make the MC approximate the EMC value during desorption process at RHI conditions (30 °C).

Free shrinkage tests under RHI conditions The specimens with 14.1% EMC were used to monitor free shrinkage deformation under the four RHI conditions. The load during collecting free shrinkage data was 0.01 N for all specimens. RH in the DMA chamber was first adjusted from 80 to 60, 40, 20, or 0% RH with the ramping rate of 2.0% RH min^{-1}. Then, the free shrinkage strain was recorded for 420-min RHI period at all four RH levels (Fig. 3a, b). MC was measured by weighing specimens at a time point and after oven dry. The time points for monitoring MC are marked by symbols in Fig. 3b. Five measurements were taken for each hygroscopic condition and orientation, and the results were shown by the average values of the five measurements. The MC evolutions during RHI conditions in Fig. 3c evidenced that the respective MCs approached the EMC values within 420 min.

MSC tests under RHI conditions The specimens with 14.1% EMC subjected to load and MC changes under the four RHI conditions were used to examine MSC during the desorption process. The experimental RH procedure was the same as displayed
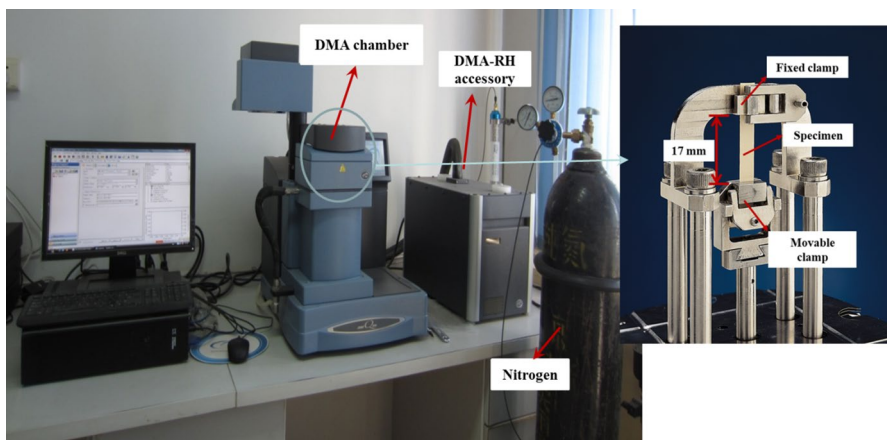
Fig. 2 Illustration of the experimental apparatus (*left*) and the mounted sample ready for tensile mode (*right*)
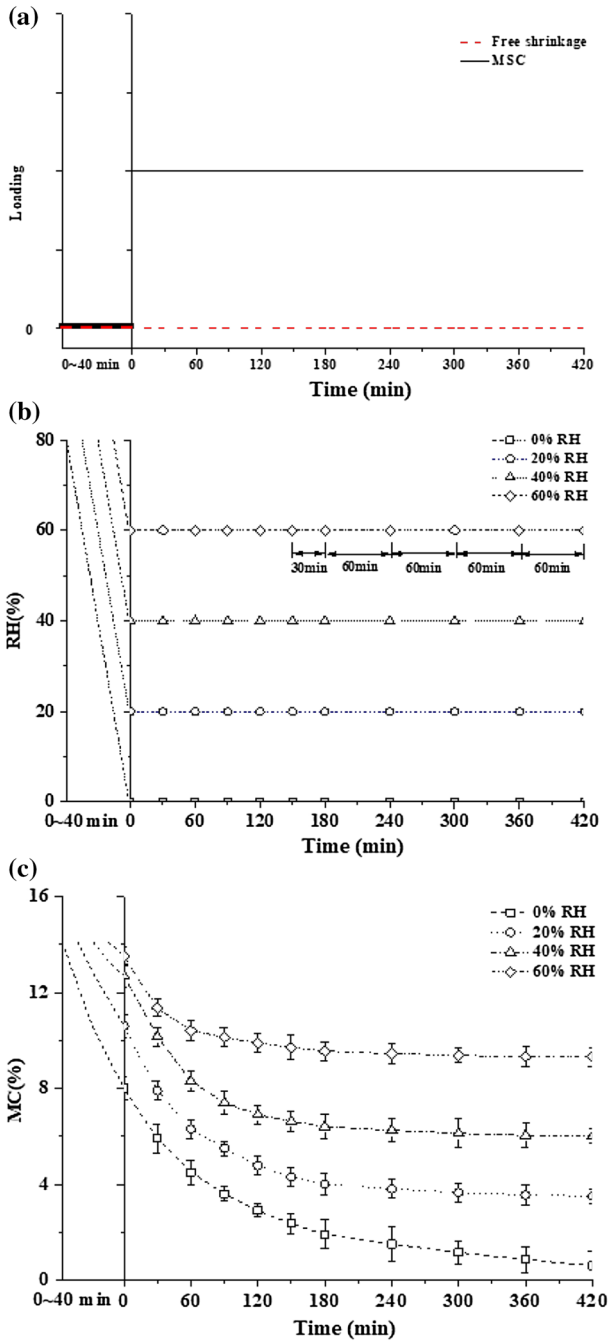
Fig. 3 Changes in load (**a**), RH conditioning (**b**), and wood MC (**c**) in free shrinkage and mechano-sorptive creep (MSC) tests

in Fig. 3b. The load was applied at the beginning of the RHI period, and then, a 420-min MSC was recorded (Fig. 3a, b). Based on preliminary stress/strain sweeps in 14.1% EMC samples under 80% RHI condition, the ultimate tensile stress of L specimen was not reached owing to the 2.1 MPa maximum stress of DMA Q800; therefore, the stress value of 1.3 MPa was selected. With regard to the *R* and *T* specimens, the stress level was set as 20% of ultimate tensile stress (1.7 MPa in *R* and 0.45 MPa in *T*), i.e., stress values were 0.34 MPa and 0.09 MPa for the *R* and *T* specimens, respectively. Five measurements were taken for each hygroscopic condition and orientation, and the results were shown by the average values of the five measurements.

VEC tests under RHI conditions The VEC tests were conducted with 0.6, 3.5, 6.0, and 9.3% EMC under 0, 20, 40, and 60% RHI conditions, respectively. The stress for VEC tests is the same as for MSC tests. Five measurements were taken for each RHI condition and orientation, and the results were shown by the average values of the five measurements.

Results and discussion

Orthotropic free shrinkage

The MC evolution during the RHI period is presented in Fig. 3c. Moisture loss below the fiber saturation point is always accompanied by dimensional changes, i.e., by free shrinkage (Fig. 4). The standard deviation of the free shrinkage was approximately 2% of the average values for each hygroscopic condition and orientation. The values of free shrinkage strain have a minus sign here to indicate the direction. The free shrinkage strain increased during all four RHI periods. The lower the RH level, the higher the free shrinkage strain irrespective of grain orientation. Higher reduction in MC resulted in greater changes of free shrinkage strain.

The orthotropic shrinkage is visible in Fig. 4. To understand the orthotropic shrinkage behavior, the ratios of *R* to *L* shrinkage (S_R/S_L), *T* to *L* shrinkage (S_T/S_L), and *T* to *R* shrinkage (S_T/S_R) determined at the end of RHI segments are listed in Table 1. Note that the *L* shrinkage was quite low; *T* shrinkage was 1.72–2.76 times higher than that of the *R* shrinkage. The orthotropic properties are highly dependent on the interactions among cell wall components. The wood cell wall can be viewed as a fiber composite system by cellulose microfibrils (CMFs) and lignin–hemicellulose matrix (Salmén 2004; Peng et al. 2017; Lu et al. 2018). The CMFs, which dominate the mechanical properties of *L* specimen, are by orders of magnitude stiffer than the matrix and largely unaffected by water desorption, i.e., they do not shrink (Schulgasser and Witztum 2015). Therefore, the CMFs restrict the shrinkage in the *L* direction. There is a large body of literature concerning the studies of the mechanisms governing the differential shrinkage behavior between the *R* and *T* specimens, which can be subdivided into three groups: the interaction between earlywood and latewood (Pentoney 1953; Krzemień et al. 2015); restriction by ray tissues (Taguchi
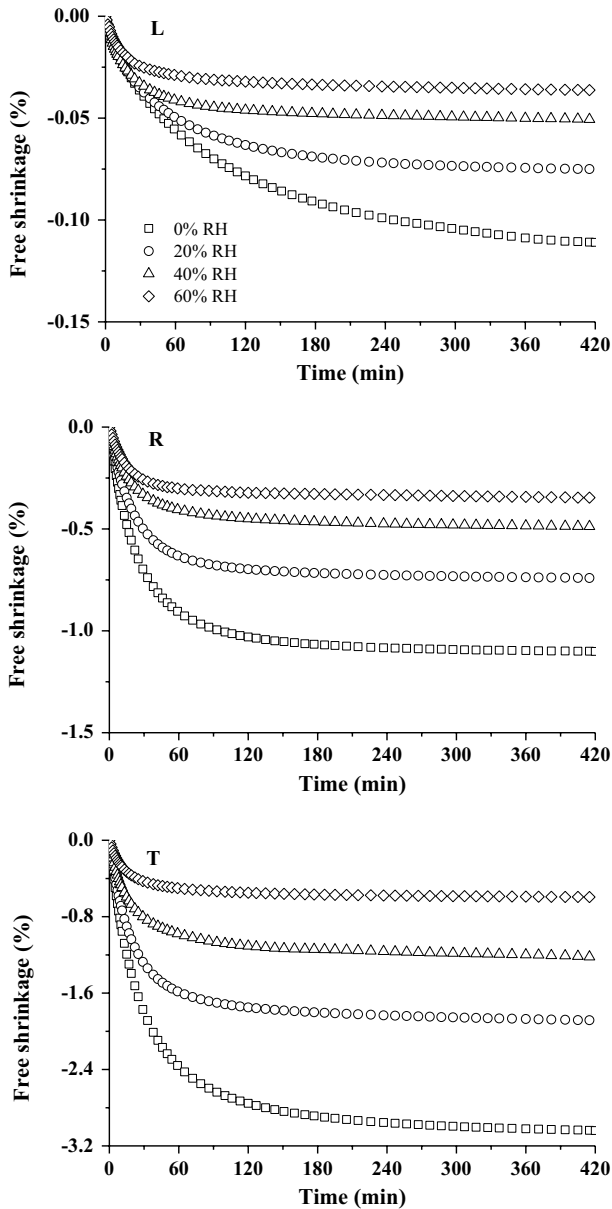
Fig. 4 Changes in free shrinkage during RHI periods (0%, 20%, 40%, and 60% RH) for *L*, *R*, and *T* specimens

et al. 2011; Bonarski et al. 2015); and differences in microfibril angle in the S2 layer (Skaar 1988; Gu et al. 2001; Bonarski et al. 2015).

The lower the RH level, i.e., the larger the MC decrement, the greater are the S_R/S_L, S_T/S_L, and S_T/S_R ratios. The S_R/S_L, S_T/S_L, and S_T/S_R increased by 3.8, 67.0, and

**Table 1** Variation in S_R/S_L, S_T/S_L, and S_T/S_R ratios with respect to RH

Parameters	RH (%)			
	0	20	40	60
S_R/S_L ratio	9.92 (0.19)	9.87 (0.21)	9.63 (0.19)	9.56 (0.20)
S_T/S_L ratio	27.38 (0.44)	25.12 (0.32)	24.13 (0.31)	16.40 (0.21)
S_T/S_R ratio	2.76 (0.06)	2.54 (0.06)	2.50 (0.05)	1.72 (0.04)

S, free shrinkage. Subscripts indicate the orthotropic directions. Values in parentheses are standard deviation

60.9%, respectively, over the measured RH range. This result indicated that the *T* shrinkage is more sensitive to RH variation than *R* shrinkage, followed by *L* shrinkage, and confirmed the theory that the CMF is highly unaccessible to water molecules and less sensitive to the RH changes.

Orthotropic VEC and MSC

For each of orthotropic VEC and MSC tests, the specimens gave very close results: The standard deviation of the strain was no more than 3% of the average values during the whole tests. Figure 5 shows the dependence of the orthotropic logarithmic elastic strain (ln ε_0) on MC. For both VEC and MSC mode, the ln ε_0 increased with the increasing MC in all orthotropic directions. However, the ln ε_0 of MSC was lower than that of VEC, even if MC is the same. The drying history before loading (Fig. 3b, c) could contribute to the lower ln ε_0 value in MSC. Additionally, the
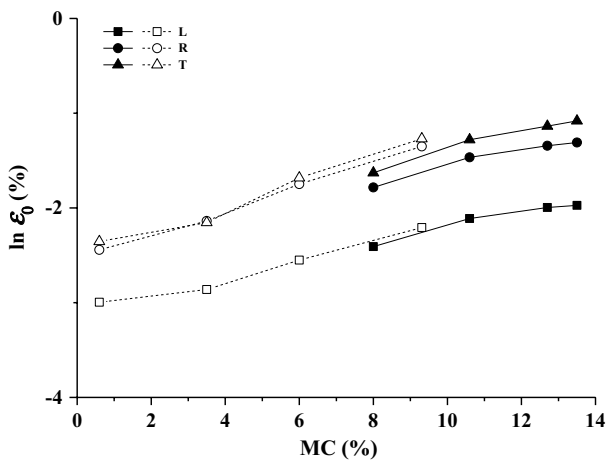

Fig. 5 MC dependency of the orthotropic logarithmic elastic strain (ln ε_0) in VEC (open symbols) and MSC (solid symbols) tests

individual $\ln \varepsilon_0$ in the three grain orientations was affected by the MC to a different degree: with an increase of 0.79 and 0.43% for $\ln \varepsilon_0^{L}$ ($\ln \varepsilon_0$ in the L direction) of VEC and MSC, respectively, 1.09 and 0.47% for $\ln \varepsilon_0^{R}$ ($\ln \varepsilon_0$ in the R direction) of VEC and MSC, respectively, 1.08 and 0.55% for $\ln \varepsilon_0^{T}$ ($\ln \varepsilon_0$ in the T direction) of VEC and MSC, respectively, over the measured MC range. Accordingly, the rise of elastic strain for the R and T specimens was more pronounced than for the L specimen in MSC test. All these findings of elastic strain are similar to the findings of the corresponding elastic compliance, regardless of grain orientation and MC (Supplementary Figure S1).

The time-dependent creep strain is dominant. Figure 6 displays the changes of the log time-dependent VEC and MSC strains during the RHI period within and between the individual orthotropic grain orientations. The negative values of MSC strain indicate that the deformation of wood opposes the load, and minus sign just expresses the direction. Both VEC and MSC strains exhibit an increasing trend
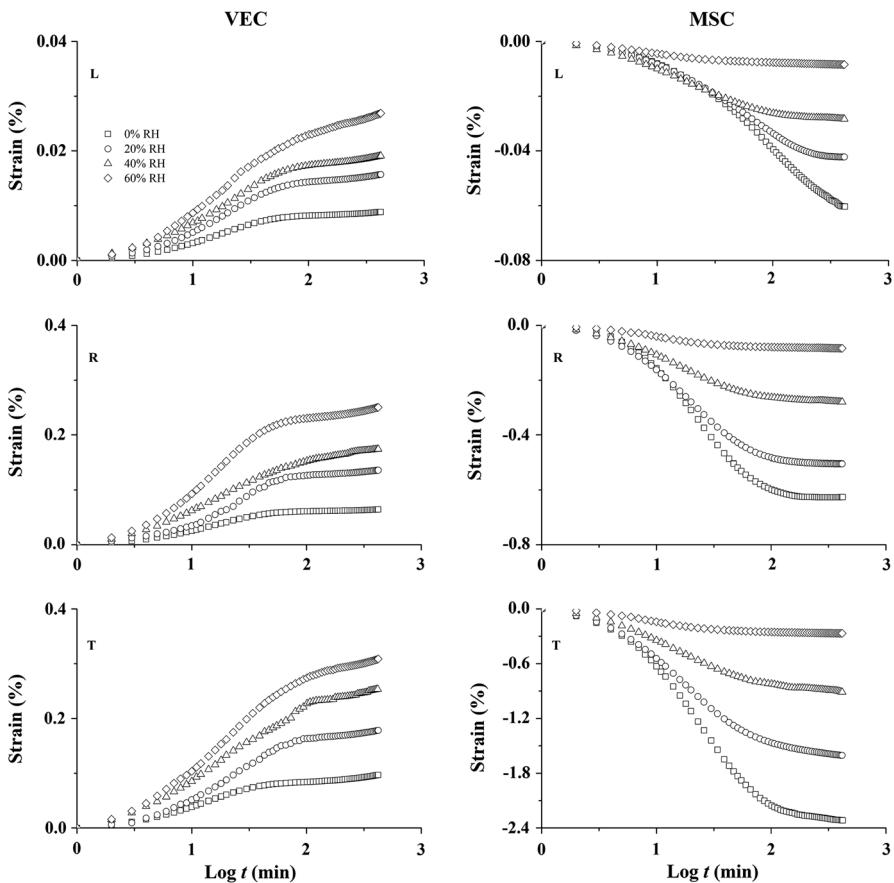
Fig. 6 Changes in VEC and MSC strains during RHI periods (0%, 20%, 40%, and 60% RH) for L, R, and T specimens

with time and a dependence on orthotropic grain orientation. As seen in Fig. 6, the curves of VEC and MSC present the expected orthotropic creep behavior: the distinctly higher strain values in transverse direction. However, the creep strain anisotropy was more pronounced in MSC tests, especially for the differential creep strain between *T* and *L* specimens. The ratio of *T* and *L* creep strains was approximately 10 and 40 in VEC and MSC tests, respectively. The creep compliance anisotropy (Supplementary Figure S2) between *T* and *L* specimens showed the same ratio as creep strain. The greater value of the ratio of *T* and *L* creep strains in MSC indicated that the MC changes could aggravate the creep anisotropy. For the MC-dependent creep behavior, it is easy to observe the MC effect on VEC (Fig. 6): a higher strain with an increasing MC (RH level) due to the plasticization effect of moisture, i.e., the rearrangement of the hydrogen bonds, RHB (Engelund et al. 2013; Zhan et al. 2019a, b). In the case of MC-dependent MSC, the logarithmic creep strain ($\ln |\varepsilon(t)|$) as a function of MC is shown in Fig. 7. These creep trajectories, which eliminate time, allow the discussion on the MC-dependent creep strain during the desorption process. Each desorption process induced a significant strain increase. However, the lines connecting each plot can be separated according to the RH level during the desorption process, irrespective of the grain orientation. This means that the amount of creep per unit change in MC depends on the drying ranges of MC. Consequently, not only the MC level but also the MC ranges affected the creep during the desorption process. The MC dependency of creep compliance trajectories (Supplementary Figure S3) was the same as creep strain. This result of MC-dependent creep behavior was consistent with previous studies (Takahashi et al. 2004, 2005).

Strain components in MSC

As can be seen in Figs. 4 and 6, the negative values of free shrinkage and MSC were found, indicating that the mechanical stress effect cannot compensate the free shrinkage. In order to analyze the contribution of free shrinkage and the mechanical stress effect to the orthotropic MSC behavior quantitatively, a "reduced strain (RS, ε_r)" obtained by subtracting the free shrinkage (ε_S) from the MSC strain is derived:

$$\varepsilon_r = \varepsilon - \varepsilon_s \tag{2}$$

The RS evolution is shown in Fig. 8. The positive values evidenced that the free shrinkage affected the MSC behavior during the desorption process. Table 2 shows the ratio of free shrinkage and MSC strain ($\varepsilon_S/\varepsilon$) determined at the end of RHI segments for *L*, *R*, and *T* specimens. The proportion of free shrinkage in MSC strain demonstrated an anisotropy (Table 2); that is, the value of $\varepsilon_S/\varepsilon$ for *T* specimen was distinctly lower than that for *L* and *R* specimens, and the $\varepsilon_S/\varepsilon$ in *L* and *R* specimens was slightly discrepant, regardless of the RH level.

Higher RS value was achieved as a function of time for all specimens (Fig. 8). The RS values at 0 and 20% RH were obviously higher than that at 40 and 60% RH, irrespective of the grain orientation. According to Eqs. (1) and (2), the RS was the result of the coupling effects between mechanical stress and MC level and MC variation in MSC behavior. Generally, a VEC reflects the coupling effects between the mechanical stress and MC level, and the MC dependency of VEC strain is
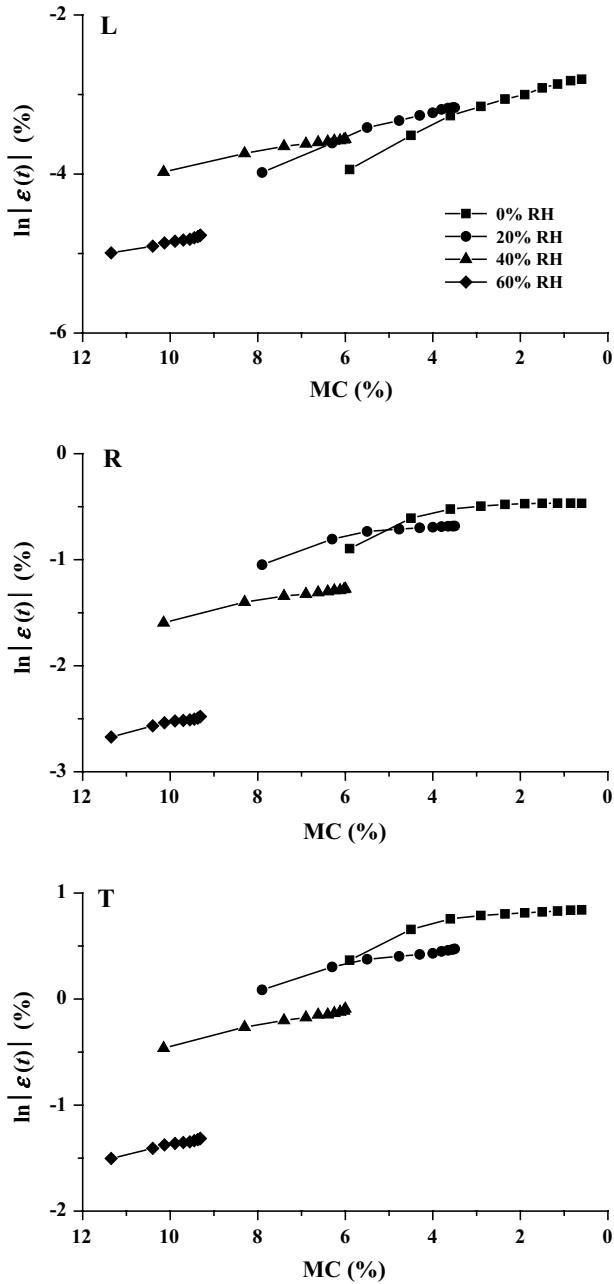
Fig. 7 Logarithmic creep strain (ln |ε(t)|) trajectories of MSC during desorption process for *L*, *R,* and *T* specimens
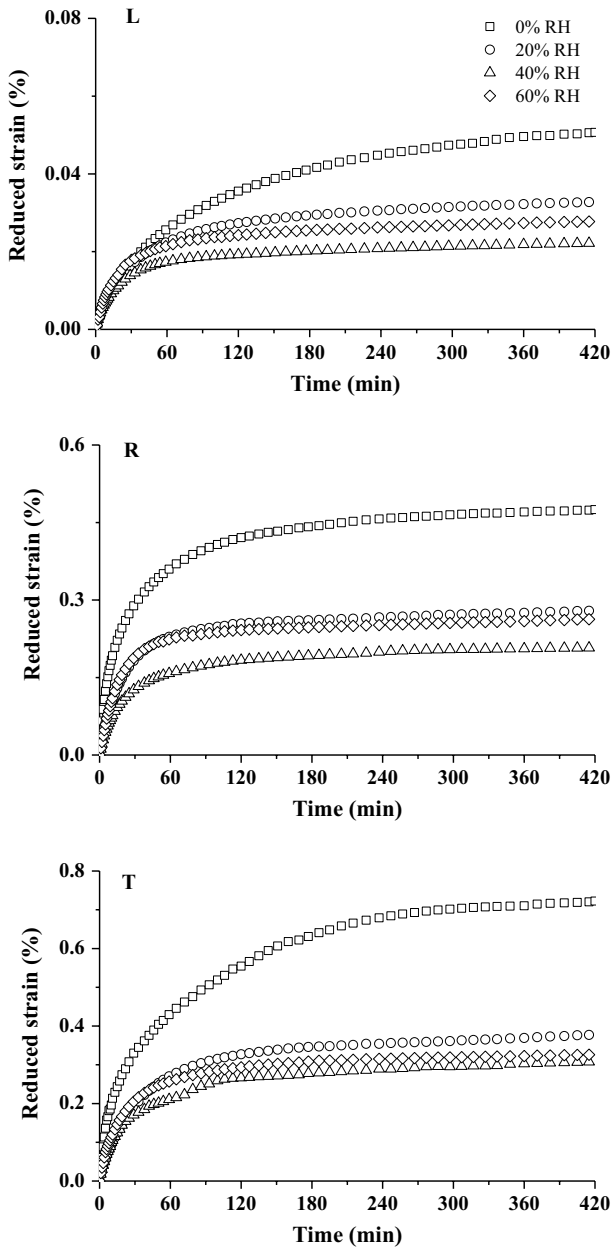
Fig. 8 Reduced strain obtained by subtracting the free shrinkage from the MSC strain during RHI periods (0%, 20%, 40%, and 60% RH) for *L*, *R*, and *T* specimens

attributed to the rearrangement of the hydrogen bonds (RHB) within the polymer network (Navi and Stanzl-Tschegg 2009; Engelund and Salmén 2012; Kaboorani et al. 2013). In addition, the MS strain corresponds to the coupling effects between

Table 2 Proportion of strain components determined at the end of RHI in MSC at four RHI levels

RHI (%)	$\varepsilon_S/\varepsilon$ (%)			$\varepsilon_{ve}/\varepsilon_r$ (%)			$\varepsilon^{ms}/\varepsilon_r$ (%)		
	L	R	T	L	R	T	L	R	T
0	183.9 (2.6)	175.7 (4.0)	131.1 (3.2)	17.5 (0.3)	13.5 (0.3)	13.4 (0.3)	82.5 (1.4)	86.5 (2.2)	86.6 (1.7)
20	177.6 (2.3)	146.5 (2.6)	117.4 (2.1)	49.3 (0.8)	48.7 (1.0)	47.2 (0.6)	50.7 (0.8)	51.3 (1.0)	52.8 (0.6)
40	188.0 (2.9)	174.2 (3.7)	128.9 (3.3)	86.0 (1.6)	83.8 (2.0)	82.4 (1.5)	14.0 (0.3)	16.2 (0.3)	17.6 (0.3)
60	426.5 (8.4)	413.3 (8.0)	221.4 (5.8)	96.7 (1.8)	95.1 (2.6)	94.5 (1.6)	3.3 (0.1)	4.9 (0.1)	5.5 (0.1)

$\varepsilon_S/\varepsilon$, proportion of free shrinkage in MSC strain; $\varepsilon_{ve}/\varepsilon_r$, and $\varepsilon^{ms}/\varepsilon_r$ are the proportions of viscoelastic creep and MS strain in the reduced strain (ε_r), respectively. $\varepsilon_r = \varepsilon - \varepsilon_S$. Values in parentheses are standard deviation

the mechanical stress and MC changes. The unstable state within the wood cell wall is associated with MS strain during MC changes (Zhan et al. 2018). Therefore, the change of the RS in Fig. 8 could be considered as a double effect composed of the RHB effect and the unstable state. More importantly, the unstable state within the cell wall can accelerate the RS strain, while RHB effect can inhibit the RS strain during the desorption process. This fact could thus explain why the RS values at 0 and 20% RH were higher than that at 40 and 60% RH, mainly because a greater unstable state contributed to the RS strain at low RH.

The unstable state could be evaluated quantitatively by MS strain (Muszyński et al. 2005, 2006; Guo 2009). Based on the dataset of VEC, the MS strain was derived from Eqs. (1) and (2) as follows:

$$\varepsilon^{ms} = \varepsilon_r - \varepsilon_{ve} \tag{3}$$

where ε_r is given in Fig. 8 and ε_{ve} is the VEC strain in Fig. 6. The evolution of MS strain is presented in Fig. 9. MS strain increased during the RHI period. Lower RH, i.e., higher reduction in MC, results in greater changes of MS strain. A lower increasing rate of MS strain appeared with increasing isohume time, indicating that the unstable state of the wood cell wall was mitigated at lower MCs toward the new EMC (Takahashi et al. 2004). The unstable state was analyzed at various RHI conditions, by a closer look at the relation of MS strain and "the difference of MC to EMC (MC_d)" (Fig. 10). MC_d was calculated:

$$MC_d = EMC_a - MC_i \tag{4}$$

where the subscript "a" designates the EMC value, and the subscript "i" denotes the corresponding MC at each RHI time point as seen in Fig. 3.

Figure 10 shows where the MS strain was inversely proportional to the isohume level, regardless of the grain orientation. In addition, here, the MS strain is dependent on the changing range of the MC during the desorption process. Higher unstable state, which contributes to MS strain, could be seen at greater MC changing ranges (Takahashi et al. 2004, 2005; Zhan et al. 2018).
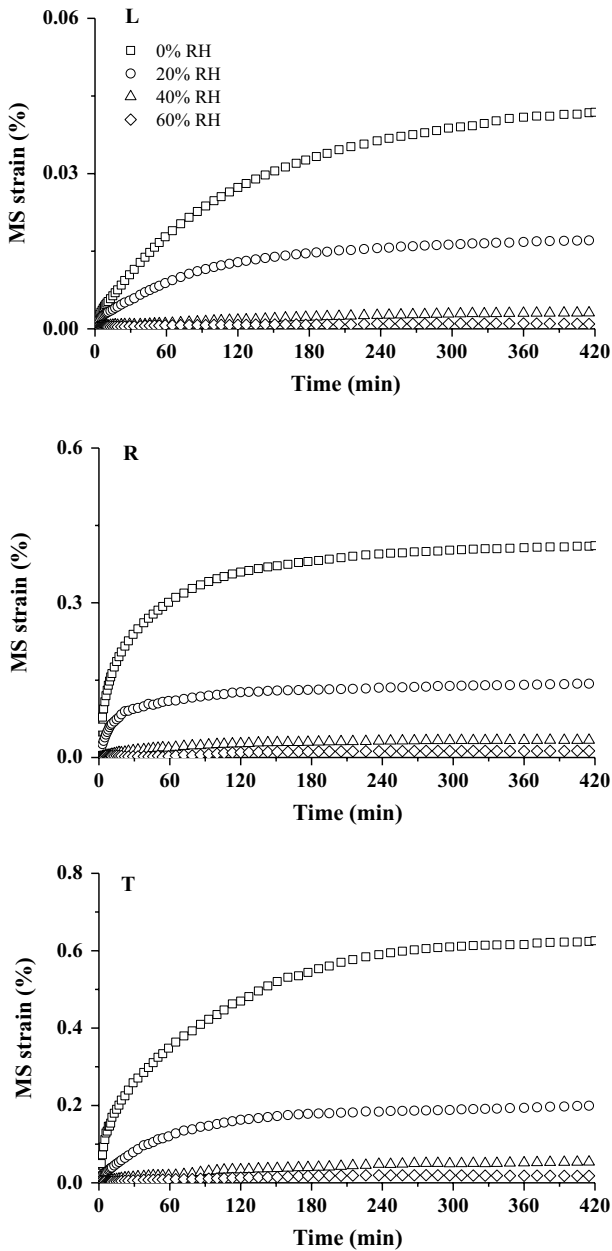
Fig. 9 Changes in MS strain during RHI periods (0%, 20%, 40%, and 60% RH) for *L*, *R*, and *T* specimens

Additionally, MS strain exhibited a distinctly orthotropic behavior at the four RHI conditions. The RH-dependent MS strain anisotropy could be evaluated at the end of RHI segment ($MC_d = 0$), as seen in Fig. 11. Lower RH level could
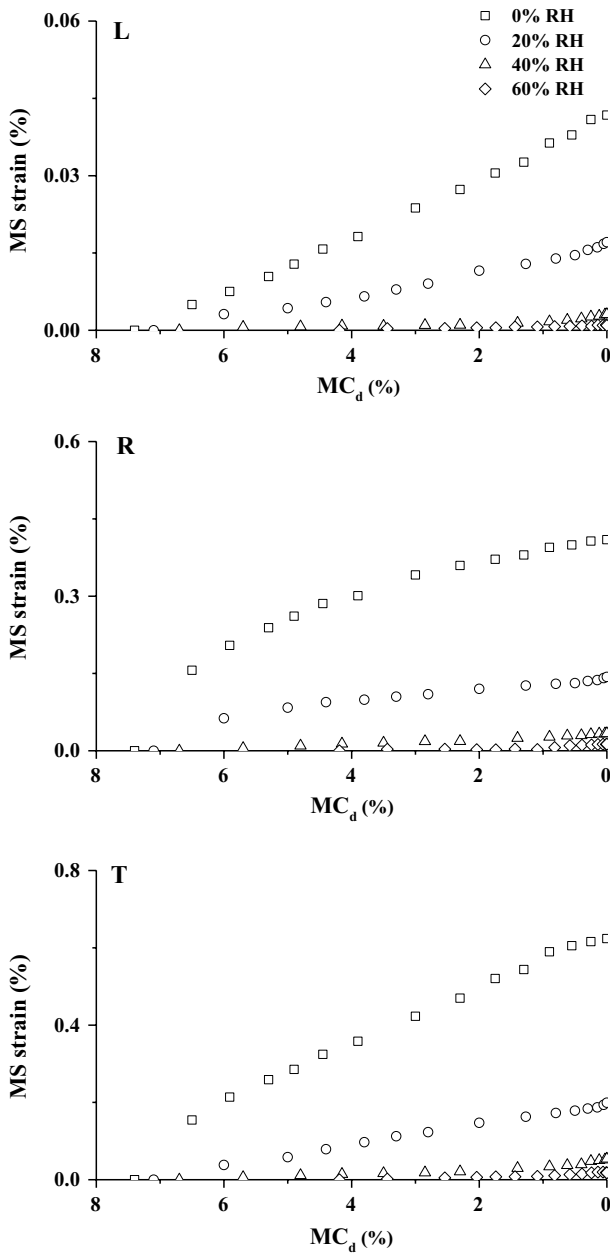
Fig. 10 Relations among MS strain and MC_d during RHI periods (0%, 20%, 40%, and 60% RH) for *L*, *R*, and *T* specimens

aggravate the differential MS strains among *L*, *R,* and *T* specimens. The reduction in MS strain for transverse specimens was more pronounced than for *L* specimen in the RH range. The results presented here proved that the unstable
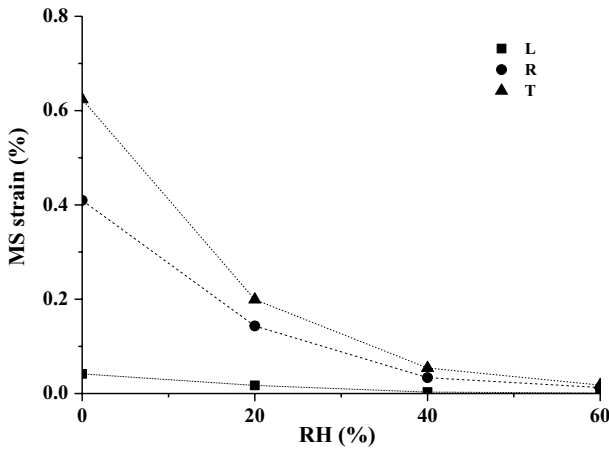
Fig. 11 RH dependency of MS strain for *L*, *R*, and *T* specimens

state of *R* and *T* specimens is affected by the RH to a higher degree than that of *L* specimen.

Based on the database of VEC and MS strains, the contribution of VEC and MS strains to RS strain can be addressed, respectively. The proportions of VEC strain in RS strain $\varepsilon_{ve}/\varepsilon_r$, and MS strain in RS strain $\varepsilon^{ms}/\varepsilon_r$ are listed in Table 2. Higher RH level, higher $\varepsilon_{ve}/\varepsilon_r$ and lower $\varepsilon^{ms}/\varepsilon_r$ are observed. This result confirmed the RHB effect enhanced the flexibility of the polymer network at higher RH level, and the unstable state contributed to the pronounced MS effect at lower RH level during the desorption process. Comparing the values among *L*, *R*, and *T* specimens in Table 2, $\varepsilon_{ve}/\varepsilon_r$ and $\varepsilon^{ms}/\varepsilon_r$ showed an opposite trend. The greater $\varepsilon_{ve}/\varepsilon$ and $\varepsilon^{ms}/\varepsilon$ values were found in *L* specimen and *T* specimen, respectively. Therefore, the coupling effects between the mechanical stress and MC changes exerted more influence on *T* specimen and had less contribution to *L* specimen.

Conclusion

The present study provides an overview on the orthotropic MSC during the desorption process in tension. The creep behaviors, VEC under constant MC conditions and MSC under varying MC conditions, were considered separately. At a given MC, the lower elastic strain in MSC tests compared to VEC tests revealed that the drying history before loading affected the elastic response. The creep anisotropy of MSC was more pronounced than that of VEC, indicating that MC changes could aggravate the creep anisotropy. In addition, the free shrinkage and MSC data offer an opportunity to calculate the contribution of free shrinkage and the mechanical stress effect on the orthotropic MSC behavior. The free shrinkage affected the deformation response during the desorption process, resulting in the negative MSC value in tensile mode. The mechanical stress can accelerate the MSC response, which is

presumed to be a result of the double effect composed of the RHB effect and the unstable state. The unstable state could be evaluated quantitatively by MS strain. The MS strain of R and T specimens was affected by the RH to a higher degree than that of L specimen. Further, the coupling effects between the mechanical stress and MC changes (i.e., unstable state) exerted more influence on T specimen and had less contribution to L specimen.

The above results provided the comprehensive data sets of the orthotropic MSC behavior at RHI conditions. However, wood suffers from different load configurations and continuous changes in humidity at large time scales in practice. Supplementary research, investigating the orthotropic MSC behavior at various humidity values closer to actual humidity conditions, could be conducted at a large time scale. Additionally, both the tensile and compressive MSC experiments can be performed to evaluate possible differences between the viscoelastic behavior in tension and compression. Moreover, a generalized Kelvin–Voigt model integrating specific hygro-lock springs will be used to model the orthotropic MSC behavior. Such model would allow interpreting the long-term response of timber structures, particularly in the case of various environmental conditions. Notably, when using a hygro-lock spring, the MC at current time determines the current "active box" within a hygro-lock spring. Thus, the dynamic vapor sorption (DVS) apparatus could be used to monitor the MC.

References

Armstrong L, Kingston R (1960) Effect of moisture changes on creep in wood. Nature 185:862–863

Bonarski JT, Kifetew G, Olek W (2015) Effects of cell wall ultrastructure on the transverse shrinkage anisotropy of Scots pine wood. Holzforschung 69:501–507

Engelund ET, Salmén L (2012) Tensile creep and recovery of Norway spruce influenced by temperature and moisture. Holzforschung 66:959–965

Engelund ET, Thygesen LG, Svensson S, Hill CAS (2013) A critical discussion of the physics of wood–water interactions. Wood Sci Technol 47:141–161

Gu H, Zink-Sharp A, Sell J (2001) Hypothesis on the role of cell wall structure in differential transverse shrinkage of wood. Holz Roh Werkst 59:436–442

Guo N (2009) Hygro-mechanical response of clear softwood specimens to compression under cyclic climate. Dissertation, Oregon State University

Hering S, Niemz P (2012) Moisture-dependent, viscoelastic creep of European beech wood in longitudinal direction. Eur J Wood Prod 70:667–670

Holzer SM, Loferski JR, Dillard DA (1989) A review of creep in wood: concepts relevant to develop long-term behavior predictions for wood structures. Wood Fiber Sci 21:376–392

Huang Y (2016) Creep behavior of wood under cyclic moisture changes: interaction between load effect and moisture effect. J Wood Sci 62:392–399

Hunt DG (1984) Creep trajectories for beech during moisture changes under load. J Mater Sci 19:1456–1467

Jiang J, Valentine BE, Lu J, Niemz P (2016) Time dependence of the orthotropic compression Young's moduli and Poisson's ratios of Chinese fir wood. Holzforschung 70:1093–1101

Kaboorani A, Blanchet P, Laghdir A (2013) A rapid method to assess viscoelastic and mechanosorptive creep in wood. Wood Fiber Sci 45:370–382

Krzemień L, Strojecki M, Wroński S, Tarasiuk J, Łukomski M (2015) Dynamic response of earlywood and latewood within annual growth ring structure of Scots pine subjected to changing relative humidity. Holzforschung 69:555–561

Lu J, Peng H, Cao J, Jiang J, Zhao R, Gao Y (2018) Application of dynamic mechanical analysis in wood science research. J For Eng 3:1–11

Montero C, Gril J, Legeas C, Hunt DG, Clair B (2012) Influence of hygromechanical history on the longitudinal mechanosorptive creep of wood. Holzforschung 66:757–764

Muszyński L, Lagana R, Shaler SM, Davids W (2005) Comments on the experimental methodology for determination of the hygro-mechanical properties of wood. Holzforschung 59:232–239

Muszyński L, Lagana R, Shaler SM (2006) Hygro-mechanical behavior of red spruce in tension parallel to the grain. Wood Fiber Sci 38:155–165

Navi P, Stanzl-Tschegg S (2009) Micromechanics of creep and relaxation of wood. A review COST Action E35 2004–2008: wood machining–micromechanics and fracture. Holzforschung 63:186–195

Navi P, Pittet V, Plummer CJG (2002) Transient moisture effects on wood creep. Wood Sci Technol 36:447–462

Peng H, Jiang J, Lu J, Cao J (2017) Application of time–temperature superposition principle to Chinese fir orthotropic creep. J Wood Sci 63:455–463

Peng H, Jiang J, Lu J, Cao J (2018) Orthotropic mechano-sorptive creep behavior of Chinese fir during the moisture adsorption process determined in tensile mode via dynamic mechanical analysis (DMA). Holzforschung 73:229–239

Pentoney R (1953) Mechanisms affecting tangential vs. radial shrinkage. J Forest Prod Res Soc 3:27–32

Saifouni O, Destrebecq J-F, Froidevaux J, Navi P (2016) Experimental study of the mechanosorptive behaviour of softwood in relaxation. Wood Sci Technol 50:789–805

Salmén L (2004) Micromechanical understanding of the cell-wall structure. C R Biol 327:873–880

Schulgasser K, Witztum A (2015) How the relationship between density and shrinkage of wood depends on its microstructure. Wood Sci Technol 49:389–401

Skaar C (1988) Wood-water relations. Springer, Berlin

Taguchi A, Murata K, Nakamura M, Nakano T (2011) Scale effect in the anisotropic deformation change of tracheid cells during water adsorption. Holzforschung 65:253–256

Takahashi C, Ishimaru Y, Iida I, Furuta Y (2004) The creep of wood destabilized by change in moisture content. Part 1: the creep behaviors of wood during and immediately after drying. Holzforschung 58:261–267

Takahashi C, Ishimaru Y, Iida I, Furuta Y (2005) The creep of wood destabilized by change in moisture content. Part 2: the creep behaviors of wood during and immediately after adsorption. Holzforschung 59:46–53

Zhan T, Jiang J, Lu J, Zhang Y, Chang J (2018) Influence of hygrothermal condition on dynamic viscoelasticity of Chinese fir (*Cunninghamia lanceolata*). Part 2: moisture desorption. Holzforschung 72:579–588

Zhan T, Jiang J, Lu J, Zhang Y, Chang J (2019a) Frequency-dependent viscoelastic properties of Chinese fir (*Cunninghamia lanceolata*) under hygrothermal conditions. Part 1: moisture adsorption. Holzforschung. https://doi.org/10.1515/hf-2018-0208

Zhan T, Jiang J, Lu J, Zhang Y, Chang J (2019b) Frequency-dependent viscoelastic properties of Chinese fir (*Cunninghamia lanceolata*) under hygrothermal conditions. Part 2: moisture desorption. Holzforschung. https://doi.org/10.1515/hf-2018-0209

Publisher's Note Springer Nature remains neutral with regard to jurisdictional claims in published maps and institutional affiliations.